Science of the Total Environment 777 (2021) 146100

Contents lists available at ScienceDirect

Science of the Total Environment

journal homepage: www.elsevier.com/locate/scitotenv

Subsea permafrost as a potential major source of dissolved organic matter to the East Siberian Arctic Shelf

Meilian Chen [a,*], Ji-Hoon Kim [b], Yun Kyung Lee [c], Dong-Hun Lee [d,f], Young Keun Jin [e], Jin Hur [c,*]

[a] Environmental Program, Guangdong Technion - Israel Institute of Technology, Shantou 515063, China
[b] Petroleum and Marine Research Division, Korea Institute of Geoscience and Mineral Resources, 124 Gwahak-ro, Yuseong-gu, Daejeon 34132, South Korea
[c] Department of Environment & Energy, Sejong University, Seoul 05006, South Korea
[d] Hanyang University ERICA Campus, 15588 Ansan, South Korea
[e] Korea Polar Research Institute (KOPRI), Incheon 21990, South Korea
[f] Marine Environment Research Division, National Institute of Fisheries Science, 216, Gijanghaean-ro, Gijang-eup, Busan 46083, South Korea

HIGHLIGHTS

- DOM Efflux rates were estimated to be 943–2,240 g C m^{-2} yr^{-1} at the transition zone with subsea permafrost
- Efflux rates of 10–55 g C m^{-2} yr^{-1} at the remainder sites S9, S10, and S12 are 1-2 orders of magnitude lower
- The released DOM is characterized by prevailing dominance of low molecular weight (M_n < 350 Da) fractions
- Seawaters and pore waters share similar optical DOM composition at the East Siberian Shelf
- Estimated benthic efflux was ~0.7–1.0 Pg C yr^{-1} when scaled up to the entire Arctic shelf with subsea permafrost

GRAPHICAL ABSTRACT

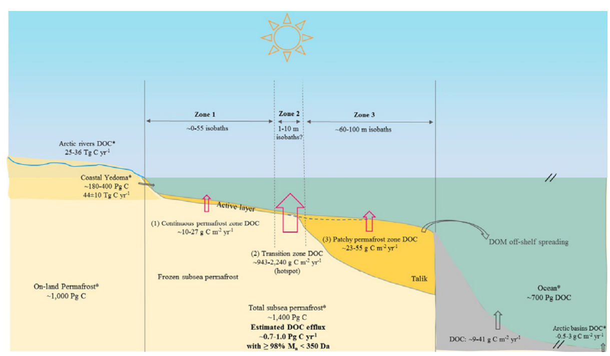

ARTICLE INFO

Article history:
Received 17 October 2020
Received in revised form 20 February 2021
Accepted 21 February 2021
Available online 28 February 2021

Editor: Manuel Esteban Lucas-Borja

Keywords:
Carbon release
Subsea permafrost
Low molecular weight fraction
Fluorescence
Benthic efflux
Arctic sediment

ABSTRACT

Arctic subsea permafrost contains more organic carbon than the terrestrial counterpart (~1400 Pg C vs. ~1000 Pg C) and is undergoing fast degradation (at rates of ~10 to 30 cm yr^{-1} over the past 3 decades) in response to climate warming. Yet the flux of organic carbon sequestered in the sediments of subsea permafrost to overlying water column, which can trigger enormous positive carbon-climate feedbacks, remain unclear. In this study, we examined the dissolved organic matter (DOM) diffusion to bottom seawaters from East Siberian Sea (ESS) sediments, which was estimated at about 943–2240 g C m^{-2} yr^{-1} and 10–55 g C m^{-2} yr^{-1} at the continuous-discontinuous transition zone of subsea permafrost and the remainder shelf and slope sites, respectively. The released DOM is characterized by prevailing dominance (≥ 98%) of low molecular weight (M_n < 350 Da) fractions. A red-shifted (emission wavelength >500 nm) fluorescence fingerprint, a typical feature of sediment/soil DOM, accounts for 4–6% and 7–8% in the fluorescence distributions of seawaters and pore waters, respectively, on ESS shelf. Statistical analysis revealed that seawaters and pore waters possessed similar DOM composition. The estimated total benthic efflux of dissolved organic carbon (DOC) was ~0.7–1.0 Pg C yr^{-1} when the estimate was scaled up to the entire Arctic shelf underlain with subsea permafrost assuming the width of continuous-discontinuous transition zone is 1 to 10 m. This estimation is consistent with the established ~10–30 cm yr^{-1} degradation rates of subsea

* Corresponding authors.
E-mail addresses: chen.meilian@gtiit.edu.cn (M. Chen), jinhur@sejong.ac.kr (J. Hur).

https://doi.org/10.1016/j.scitotenv.2021.146100

permafrost by estimating its thaw-out time. Compiled observation data suggested that subsea permafrost might be a major DOM source to the Arctic Ocean, which could release tremendous carbon upon remineralization via its degradation to CO_2 and CH_4 in the water column.

1. Introduction

The shallow Arctic shelf (seawater depth < 100 m) underlain with subsea permafrost, primarily located in the Siberian, Chukchi, and Beaufort Seas, is a seaward extension of tundra ecosystem inundated during the Holocene marine transgression occurring about 7–15 kyrs BP (Romanovskii et al., 2005). The Arctic shelf, especially the East Siberian Arctic Shelf (ESAS), has received much scientific attention due to the recent findings such as activation and degradation of old Pleistocene subsea and coastal permafrost (Vonk et al., 2012; Shakhova et al., 2017), extensive CO_2 and CH_4 bubbling and outgassing (Anderson et al., 2009; Shakhova et al., 2010), and acidification and export of $CaCO_3$ corrosive waters (Semiletov et al., 2016; Anderson et al., 2017). Considering the recent interesting reports on the above-mentioned phenomena as well as an important status of dissolved organic matter (DOM) in aqueous environment as the ubiquitous presence and the most mobile form of organic carbon, it is pressing to investigate the DOM dynamics in the seawaters and sediments of the Arctic shelf. This kind of studies can advance the current understanding of the ecosystem responses and carbon-climate feedbacks in the fast warming Arctic.

Subsea permafrost is known to contain a much larger stock of organic carbon than the on-land counterpart (1400 Pg C vs. 1000 Pg C, Soloviev et al., 1987; Tarnocai et al., 2009; Shakhova et al., 2010). Furthermore, subsea permafrost is experiencing faster erosion (at rates of ~10–30 cm yr^{-1} since 1985) and degradation than terrestrial permafrost due to the influx of salt and heat (bottom seawater temperature − 1.8–1 °C) after the inundation by seawater, which is about 12–17 °C warmer than the surface annual average temperature of on-land permafrost (Soloviev et al., 1987; Romanovskii et al., 2005; Shakhova et al., 2017). Besides thermal erosion (including geothermal flux), subsea permafrost is subject to chemical and current-induced seafloor erosion, leading to release of a large amount of organic carbon potentially as much as riverine inputs and coastal erosion (Rachold et al., 2000; Romanovskii et al., 2005; Nicolsky and Shakhova, 2010). The active seafloor thermal erosion caused meters of subsea permafrost thawing over the past three decades which is even faster than previously thought (Razumov, 2000; Romanovskii et al., 2005; Grigoriev, 2008; Shakhova et al., 2017, 2019). The subsea permafrost is continuous to the ~60 m isobath and becomes discontinuous and "patchy" at outer shelf until ~100 m isobath, where seawaters flooded this area > 12 kyrs BP and permafrost degrades the most (Romanovskii et al., 2005; Shakhova et al., 2019). Opposite to the general seaward tapering of relict permafrost trend, submerged taliks (thawed layer or column of permafrost), caused by top-down and/or bottom-up heat and salt intrusion, deepen seaward on the Arctic shelf (Osterkamp and Harrison, 1985; Rachold et al., 2007).

Despite the pivotal importance of the fast thawing Arctic subsea permafrost in terms of global carbon budget and climate, studies on benthic flux of DOM from shallow Arctic sediments underlain with subsea permafrost are surprisingly rare. Furthermore, DOM is the dominant form of organic matter in the Arctic major rivers and seas (>90%, Lobbes et al., 2000; Salvadó et al., 2016). The main objectives of this study are to (1) quantitatively estimate benthic efflux of DOM from the shallow Arctic shelf sediments underlain with subsea permafrost, and (2) characterize the DOM of the sediment pore water and overlying seawaters to better understand the benthic efflux. To achieve these goals, we utilized bulk dissolved organic carbon (DOC), ultraviolet-visible spectroscopy (UV–Vis), 3D fluorescence excitation emission matrix coupled with parallel factor analysis (EEM-PARAFAC), and size-exclusion chromatography coupled with organic carbon detector (SEC-OCD). We selected the East Siberian Sea (ESS) as the study site since it is well-known as a hotspot of greenhouse gas venting and subsea permafrost destabilized region (Vonk et al., 2012; Anderson et al., 2009; Shakhova et al., 2010, 2017).

2. Methods

2.1. Sites description

The ESS is one of the largest (area of 987 × 10^3 km^2), the widest (a 2400 km coastline), the shallowest (mean seawater depth of ~52 m), the most covered by sea-ice, and the least-explored Arctic marginal seas (Fig. 1 and Fig. S1), which is mostly underlain with subsea

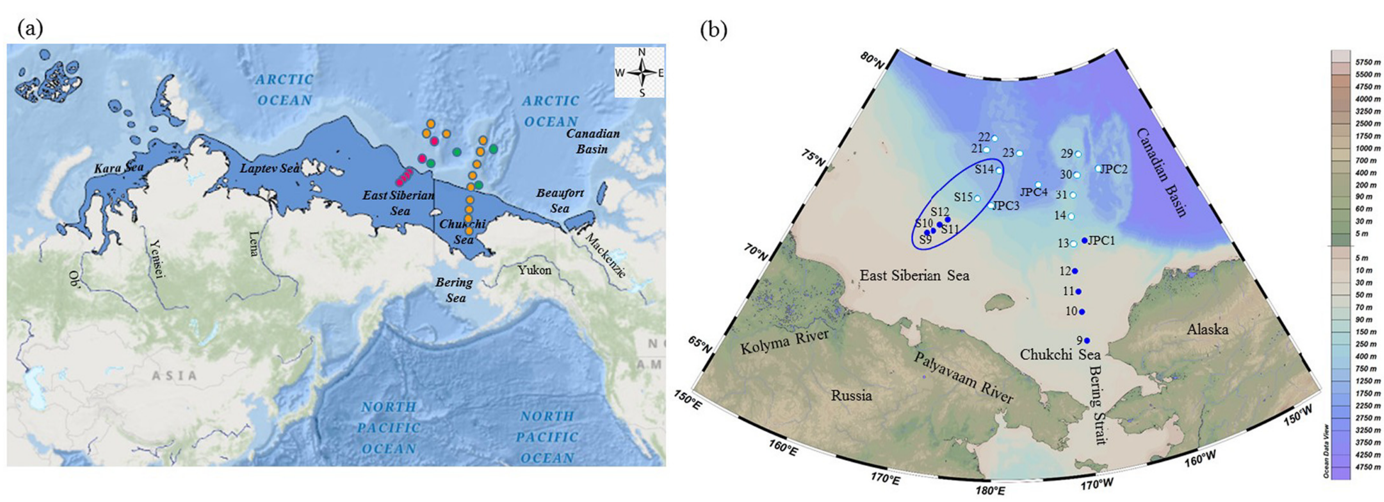

Fig. 1. (a) Sampling sites (red circles numbered S9 to S15) of seawater and pore water in the East Siberian Sea (ESS) in the mid-September 2019. Green and orange circle sites are from prior studies in the vicinity (Chen et al., 2016, 2017, 2018). Subsea permafrost layer is highlighted with blue colour with a total area of 2.5 × 10^6 km^2 (Angelopoulos et al., 2020). Map was created with ArcGIS software (Esri, USA). (b) Enlarged map of sampling sites produced with ODV software (Schlitzer, 2020). Blue circles were ice free and white circles were sea ice-covered at time of sampling.

permafrost and undergoing fast warming (Stein and Macdonald, 2004; Dmitrenko et al., 2011; Rivchter-Menge et al., 2019). Marine primary production (15–30 Mt C yr^{-1}, Mt = Tg = 10^{12} g) was thought to serve as a dominant source of organic matter to the ESS even though there are significant terrestrial inputs from coastal erosion, riverine runoff, eolian deposition, and underground runoff, which account for about 2.2 Mt, 1.9 Mt, 0.16 Mt, and 0.1 Mt of organic carbon, respectively (Sakshaug, 2004; Vetrov and Romankevich, 2004, 2011). However, a more recent study estimated that coastal Yedoma erosion actually contributes more organic carbon than prior estimations in response to climate warming (~44 ± 10 Tg C yr^{-1} along the ~7000 km ESAS coastline, Vonk et al., 2012). The inputs from subsea permafrost have been largely neglected previously. The ESS is affected by a high ice algae primary productivity (3.5–4.7 Mt C yr^{-1}) rather than by open water primary productivity compared to other Arctic seas (Vetrov and Romankevich, 2011). There are two distinct hydrological provinces for the seawaters in the ESS with transitional frontal zones between nutrient-rich Pacific-derived waters inflowing from the Bering Strait and Arctic shelf waters. The frontal zones shift between roughly 160° E (Az-mode) and 172° E (Zn-mode), depending on the atmospheric circulation regimes switching between anticyclonic circulation (i.e., high pressure in the central Arctic, ~160° E) and cyclonic circulation (i.e., low pressure in the central Arctic, ~172° E, Semiletov et al., 2005; Dmitrenko et al., 2005). Major rivers discharging into the ESS are the Kolyma and Indigirka rivers (~103 km^3 yr^{-1}, http://rims.unh.edu/). In addition, the Lena River freshwater plume can reach the region of ~165° E–180° E, which is carried by the low salinity eastward Siberian Coastal Current (SCC, Nikiforov and Shpaikher, 1980). DOC concentrations in the outer shelf of ESS have been reported to be about 724–938 and 935–2170 μg L^{-1} in the eastern and western sections, respectively, in summer (Salvadó et al., 2016). However, large spatiotemporal variations were observed in these studies.

Although marine autochthonous productivity was thought to be the dominant source of organic matter to water column of the ESS, the Pleistocene ice-bearing permafrost-derived source prevails in sedimentary organic matter throughout the broad shelf (~57%, Vonk et al., 2012, 2014). Besides fluvial runoff of permafrost-derived organic matter, erosion of the ancient organic carbon-rich Yedoma outcropping along the 2400 km shoreline of the ESS has caused coast retreat at rates of ~0.5–10 m yr^{-1} (Rachold et al., 2004; Lantuit et al., 2012; Günther et al., 2013). The Arctic rivers and coastal Yedoma are estimated to input 25–36 Tg C yr^{-1} of DOC and 44 ± 10 Tg C yr^{-1} of organic carbon to the coastal Arctic Ocean, respectively (Raymond et al., 2007; Vonk et al., 2012). Subsea permafrost is presumed to be another source of organic matter to the ESS of the Arctic ocean but there was no study to provide the quantitative and supporting evidence. Sedimentation rates in the ESS are about 0.11–0.16 mm yr^{-1} offshore with sediment core depth of ~1 m archiving the entire Holocene epoch (~10,650 yrs BP, Aksenov, 1987; Vonk et al., 2012).

2.2. Sampling and onboard analyses

The sampling sites are primarily located in the eastern section of the ESS between.

168.8° E and 180° E (Fig. 1 and Fig. S1). Seawater and pore water sampling were performed along a transect from shallow to deep water depth in the ESS constituted six sites (S9, S10, S11, S12, S15 and S14 in Fig. 1b) during the ARA010C Expedition in mid-September 2019. Thirty seawater samples were collected in this transect using a CTD/rosette system holding 24-10L Niskin bottles (SeaBird Electronics, SBE 911 plus) in the Korean icebreaker *R/V* ARAON, which covered surface to bottom seawater at each site (Table S1). The CTD recorded the basic data such as salinity, temperature, and chlorophyll fluorescence signal, and dissolved oxygen while it descended to the seafloor.

The sediment cores were recovered by multi-corer. The length of all cores is shorter than 0.6 m. Pore waters were extracted for about 1 h using Rhizon samplers at 4–12 cm intervals by perforating holes in the sediment core liner. Six pore waters at each site were collected in 25 ml acid-prewashed syringes (Table S2). The extracted pore water was collected in 25 ml acid-prewashed syringes.

The collected seawater and the pore water samples were filtered through 0.20 μm disposable polytetrafluoroethylene filters and were transferred into HCl-prewashed high-density polyethylene bottles for the DOM analyses. The salinity measurements for pore waters were taken onboard using a temperature-compensated Fisher hand-held refractometer. The International Association of Physical Sciences of the Oceans (IAPSO, 34.99 psu) standard was used for the calibration of salinity.

2.3. SEC-OCD measurements

Molecular size distributions of DOM samples (i.e., seawater and pore water) were measured using a high-performance liquid chromatography system (S-100, Knauer, Berlin, Germany) equipped with an organic carbon detector (OCD), which is located at Sejong University (Seoul, South Korea). Representative samples (surface water, bottom water, pore water from surficial and deeper sediments) were chosen from the sites along a shelf-slope gradient for SEC-OCD measurement. Different size molecules were separated through a size exclusion column (250 mm × 20 mm, TSK HW 50S) installed in the system. The detailed information for the analysis is available elsewhere (Huber et al., 2011). Five different molecular weight (MW) fractions, such as biopolymer (BP), humic substances (HS), building blocks (BB), low molecular weight acids (LMA), and low molecular weight neutrals (LMN), were quantified based on an established guideline (Huber et al., 2011) and the in-built software.

The fractions obtained can be utilized to assess the molecular size and sources of DOM.

2.4. DOC, UV–Vis and EEMs measurements

The DOC concentrations were measured with a total organic carbon analyzer.

(Shimadzu TOC-VCPH, Japan) after sample acidification as non-purgeable organic carbon. The UV–Vis absorption spectra were scanned from 200 nm to 800 nm using a spectrophotometer (model: Shimadzu 1800, Japan). EEMs were obtained using a 3D fluorescence spectrophotometer (model: Hitachi Inc., Japan) with excitation/emission wavelengths of 200–500/280–550 nm and a scanning speed of 12,000 nm min^{-1}. Excitation and emission steps were set at 5 nm and 1 nm, respectively. Instrument automatic correction was on during measurements. The optical properties and associated indicators, explained in the footnotes of Table S1, can be used to trace the sources and composition of DOM.

2.5. Benthic flux estimation using Fick's first law

In diffusion-dominated systems, benthic flux can be estimated with the following equation (Eq. (1)) assuming sediment resuspension and advections are negligible (Burdige and Martens, 1990):

$$J = \phi_o \times D_s \times (\partial C/\partial z)_o \tag{1}$$

where the symbols stand for: J = diffusion flux, ϕ_o = surface sediment porosity, D_s = diffusion coefficient at water-sediment interface, $(\partial C/\partial z)_o$ = the concentration gradient at the water-sediment interface. In this study, under an assumption of a linear concentration gradient, $(\partial C/\partial z)_o$ was calculated with $\Delta C/\Delta x$ in which $\Delta C = C_{\text{sediment pore water at 1–2 cm}} - C_{\text{overlying bottom water}}$ and Δx is the mid-point of the core section.

In order to constrain diffusion coefficients for different MW fractions, the following empirical equation (Eq. (2)) was adopted (Burdige et al., 1992):

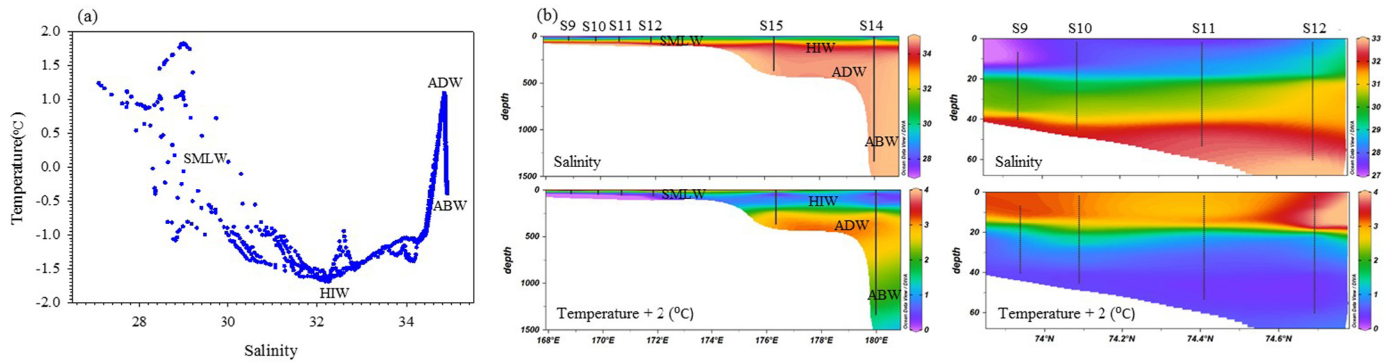

Fig. 2. Temperature-salinity diagram (a) displaying water masses: Surface Mixed Layer Waters (SMLW), Halocline Intermediate Water (HIW), Atlantic Deep Waters (ADW, seawater depth ~ 350–900 m), and Arctic Bottom Waters (ABW, seawater depth > 900 m) (Woodgate et al., 2005) and section plots of seawater temperature and salinity (b). Note that temperature scale has been added 2 °C to get positive values in order to plot graphs using ODV software (Schlitzer, 2020).

$$\text{Log D}^{\circ} = 1.72\text{–}0.39 \times \log \text{MW}_{\text{SEC-OCD}} \tag{2}$$

where D° = free solution diffusion coefficient at 25 °C in distilled water and $MW_{SEC\text{-}OCD}$ denotes molecular weight estimated by SEC-OCD measurements.

2.6. Data handling and statistics

The Napierian absorption coefficient a_{254} and a_{320} of chromophoric DOM (CDOM) were calculated as follows (Blough and Del Vecchio, 2002):

$$a_\lambda = 2.303 \times A_\lambda / L \tag{3}$$

where A_λ is the optical density and L is the pathlength of cuvette. For fluorescent DOM (FDOM), several post-acquisition corrections were made for EEMs, which included Milli-Q water blank subtraction, inner filter effect correction using UV–Vis data, and Raman unit (RU) normalization. In order to produce a PARAFAC model with more components, additional EEMs data from prior studies in the ESS and neighboring Chukchi Sea were combined to those of the current study. Some outlier EEMs with a strong elongated signal were excluded, which was presumably created by ice algae bloom. The related discussion is stated in Section 3.1 below. The PARAFAC modeling was performed in MATLAB R2020a. Principal component analysis (PCA) was carried out using R software via *vegan* package (https://www.r-project.org/).

3. Results and discussion

3.1. Extremely high AOU in ESS seawaters

The temperature-salinity diagram showed the existence of four types of water masses for the samples collected in this study (Fig. 2, Woodgate et al., 2005), namely, low salinity Surface Mixed Layer Waters (SMLW), Halocline Intermediate Water (HIW), warm Atlantic Deep Waters (ADW, seawater depth = ~350–900 m), and Arctic Bottom Waters (ABW, seawater depth > 900 m). ADW is present at sites S14 and S15. ABW is dominant at site S14 where water depth is 1350 m.

Raw data measured by in situ fluorescence sensor showed relatively high signals at the bottom of shallow site S9 (water depths <50 m, Fig. 3, Table S1), implying potential higher benthic chlorophyll *a* (chl-*a*) at the shallower shelf of the ESS in fall season. Very high apparent oxygen utilization (AOU) was seen in the ESS seawaters (~227–370 umol kg^{-1}, Table S1). High AOU indicates high organic matter oxidation rates. On the other hand, the relatively high AOU throughout the water column at ice-edge sites S14 and S15 can be explained by ice algae bloom. Lasting near-ubiquity ice-edge blooms have been reported in the Arctic Ocean (Perrette et al., 2011).

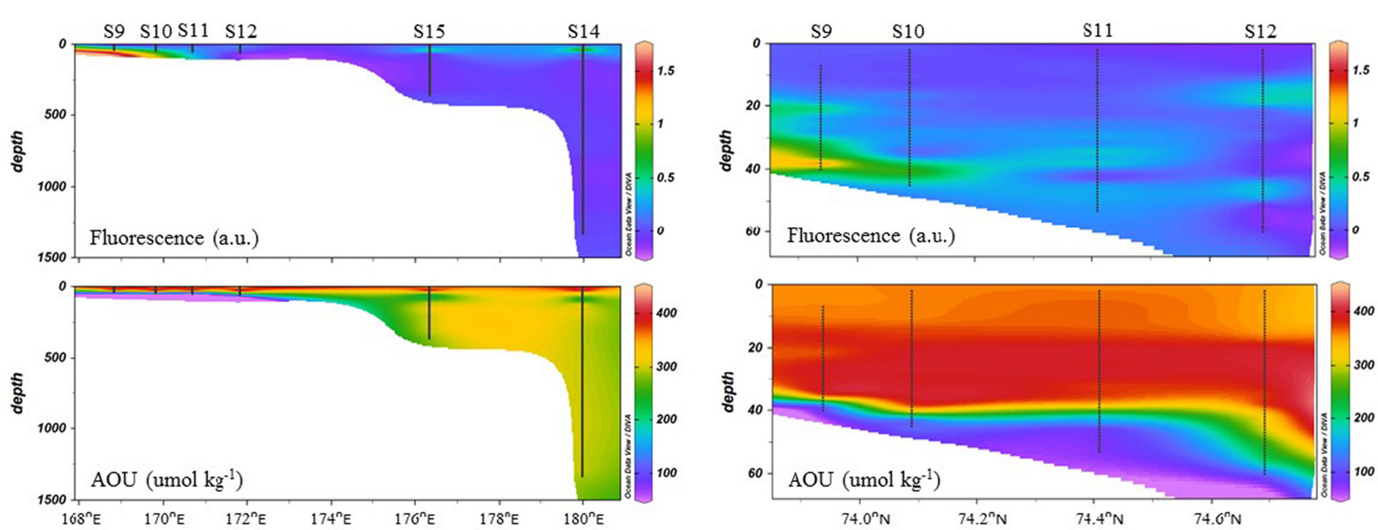

Fig. 3. Section plots of raw fluorescence data and apparent oxygen utilization (AOU) measured by in situ sensors along a shelf-slope gradient. Low AOU levels were observed close to bottom water at shelf sites and below the surface water at the slope sites.

3.2. Humic-like FDOM fingerprints and off-shelf spreading of DOM in the eastern ESS

Six FDOM components, including four humic-like and two protein-like components, were identified from PARAFAC modeling (Fig. 4-a). In addition, there was an accumulation of an elongated protein-like signal C7 in pore waters at slope sites S14 and S15, which was also observed in the Arctic during summer and fall ice-edge algal blooms (Chen et al., 2017; Chen et al., 2021). The EEMs with this C7 signal were excluded in PARAFAC modeling as outliers to facilitate the split-half validation. The humic-like fingerprints were obvious on the shelf in the East Siberian-Chukchi Seas environments, with terrestrial humic-like components $C_{<260(345)/445}$, $C_{285(370)/>500}$, and $C_{<260/430}$ accounting for 20–30% totally (12–16%, 4–8%, and 4–6%, respectively, Table S1 and S2). Marine/microbial humic-like $C_{310/400}$ accounts for 8–16% on the East Siberian-Chukchi shelf while it accounts for 28–47% in the seawaters on the slope sites of S14 and S15. It was observed that Arctic bottom water (ABW) at site S14 contains no to little terrestrial humic-like $C_{285(370)/>500}$ and $C_{<260/430}$. The observation is reasonable because the former is a red-shifted component usually enriched in reduced environments of soils/sediments while the latter is a proxy of photo-degradation. Similar to the neighboring Chukchi Sea (Chen et al., 2018), there was a trend of off-shelf spreading of DOC, CDOM, and humic-like FDOM in the eastern ESS (Fig. 4-b).

3.3. Benthic venting of LMW-dominated DOM from continuous-discontinuous transition zone of the subsea permafrost

The core lengths ranged from 31 cm below seafloor (cmbsf) at site S9 to 44 cmbsf at site.

S15 (Table S2), corresponding to ~2000–4000 yrs BP based on the estimated sedimentation rate of 0.11–0.16 mm yr^{-1} in this region (Vonk et al., 2012). It was surprising to observe that the downcore profiles of pore water FDOM were rather constant while DOC and CDOM decreased at site S11, which contrasted with the profiles of CDOM and FDOM accumulation with depth typical for Arctic and other marine sediments that are not underlain with subsea permafrost (Fig. 5, Figs. S5–S7, Chen et al., 2016). Furthermore, extremely high DOC concentrations of 395 and 218 mg-C L^{-1} were observed in shallow sediment pore waters at depths of 1 and 6 cmbsf at site S11 (seawater depth = 59 m). In fact, these high DOC levels have never been seen in any natural marine environments except for marine systems with subsea permafrost (up to 240 mg-C L^{-1}, Overduin et al., 2015), which we will discuss in detail below. Much higher DOC concentrations (up to 660 mg-C L^{-1}) are also found below the permafrost table in a Greenland wetland (Jessen et al., 2014). It is noteworthy that the average DOC concentrations of seawaters at site S11 are also the highest (2.0 ± 0.3 mg-C L^{-1}, Table S1) among the investigated sites. The pore waters concentrations at the remainder sites range from 8.4 ± 1.2 mg-C L^{-1} at slope sites S14 and S15 to 14.5 ± 3.3 mg-C L^{-1} at shelf site S12, which were comparable to the high end of ~10.5 mg-C L^{-1} observed in the pore waters at the Arctic Fram Strait (Rossel et al., 2020).

DOC levels at site S11 decreased sharply downcore with DOC reaching 10.0 mg-C L^{-1} at a depth of 20 cmbsf, coincident with salinity increase from 34.5 to 35.0 and CDOM absorption coefficients a_{320} and a_{254} plummet from 153 m^{-1} to 20 m^{-1} and ~ 444 m^{-1} to 40 m^{-1}, respectively (Fig. 5). The coincident sharp decreases of DOC and CDOM levels suggested a significant fraction of DOC is optically active. The salinity of pore water might dip a little after presumed subsea permafrost thaw due to mixing with the bottom water with lower salinity (~ 33 psu, Rachold et al., 2007). Indeed, extremely high DOC concentrations in sediment pore waters (~7–395 mg-C L^{-1}) combined with strong signals of terrestrial humic-like FDOM (~20–30%) in both seawaters and pore waters on the shelf point to a scenario of subsea permafrost-derived DOM rather than ordinary marine sediment mineralization. Although we are unable to tease apart DOC contributions from

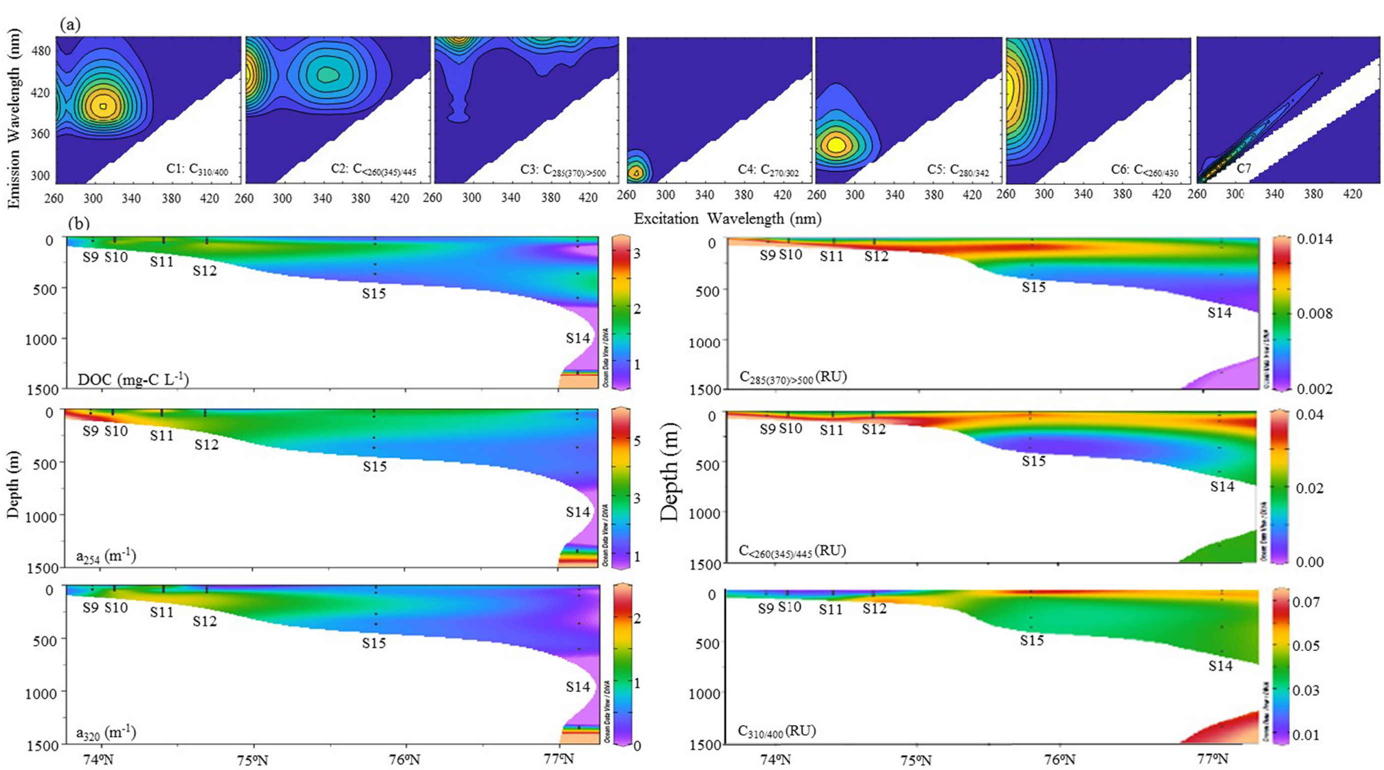

Fig. 4. (a) Contour plots of six EEM-PARAFAC components (C1-C6) identified for FDOM using a combined dataset in the East Siberia Sea and in the neighboring Chukchi Sea after excluding pore water EEMs from sites S14 and S15 which uniformly displayed a strong elongated signal (C7: ex/em maximum at 280/310 nm), potentially produced by ice algal bloom, which was also observed during phytoplankton blooms in the high Arctic (Chen et al., 2017, 2021). (b) Sections plots of DOM parameters display off-shelf spreading (~50–200 m depth) of bulk DOC, absorption coefficients, and humic-like FDOM.

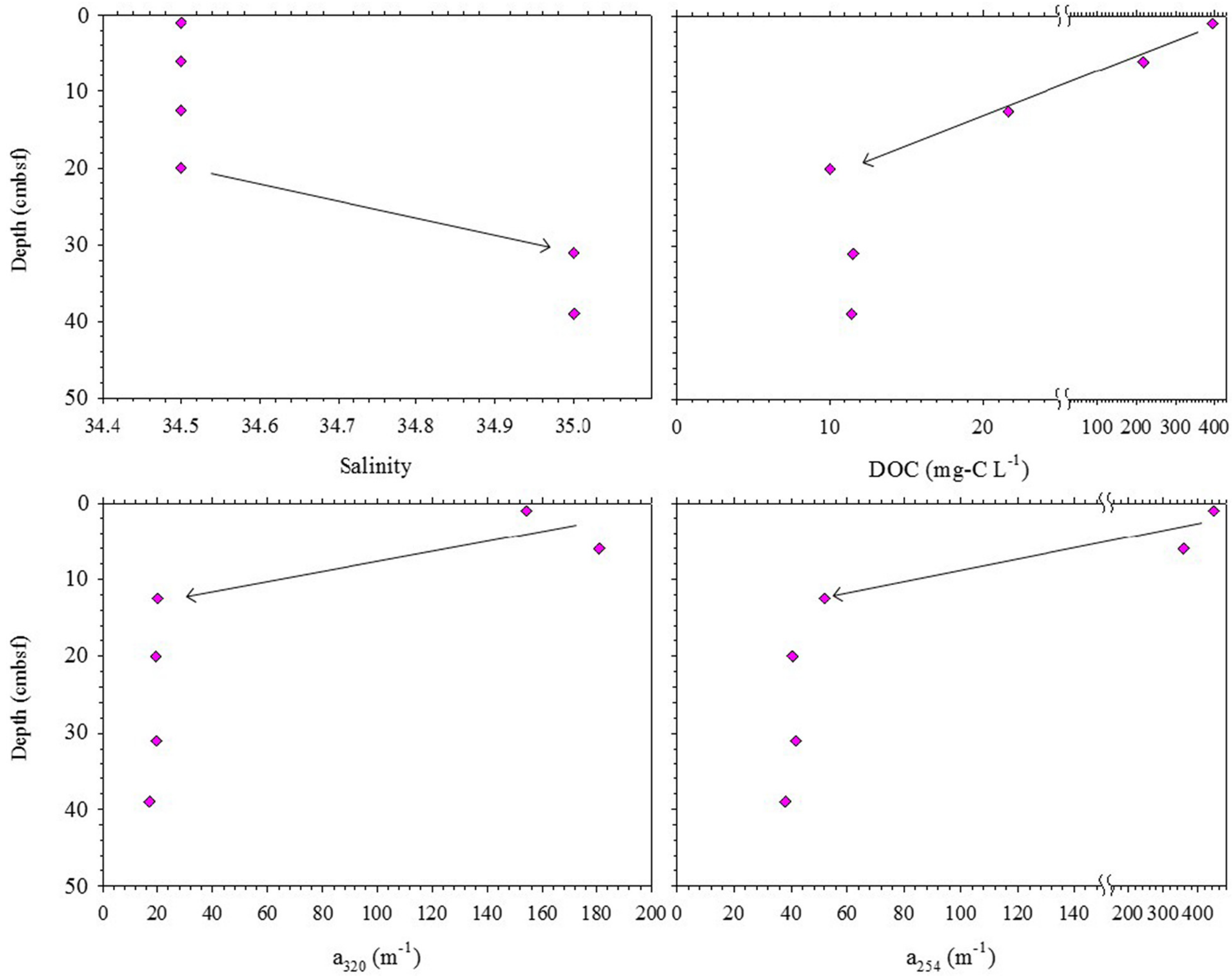

Fig. 5. Downcore profiles of salinity, bulk DOC, and absorption coefficients for sediment pore waters at site S11 (located in the continuous-discontinuous transition zone of subsea permafrost) from the ESS of Arctic Ocean. Note extremely highly DOC and CDOM at surface sediment.

ordinary benthic sediment versus degrading subsea permafrost at present, we infer that contribution from ordinary benthic sediment mineralization is minor considering that the studying sites are far offshore instead of nearshore where riverine sediment inputs may play a bigger role. Cross-shelf transport of sediments takes thousands of years and can remove the majority of terrestrial organic carbon (Bröder et al., 2018). Furthermore, the DOC flux rates from ordinary Arctic sediments are orders of magnitude lower than those from the ESAS sediments in this study (maximum values of 10 vs. 2240 g C m^{-2} yr^{-1}, Table 1). Meanwhile, coincident decline downcore trend of a photo-product proxy $C_{<260/430}$ and molecular weight index S_R and increase of aromaticity indicator a^*_{254} suggested smaller size DOM with relatively lower aromaticity are released to surficial sediment pore waters after subsea permafrost thaw (Fig. S7 and S8), which were in line with LWM-dominated DOC distribution from the SEC-OCD results later. The DOC downcore profiles are relatively stable at other sites fluctuating between ~7 to 14 mg-C L^{-1}, except for site S12 (seawater depth = 65 m) reaching ~20 mg-C L^{-1} at surface sediment pore water. The site

Table 1
DOC concentrations of pore water and benthic flux of DOC and CDOM in the Arctic Ocean. Positive values denote efflux from sediments and vice versa.

Site	Seawater Depth (m)	Location	Subsea Permafrost	DOC (mg-C L^{-1}) at 1–2 cmbsf	DOC (g C m^{-2} yr^{-1})	CDOM ((m^{-1} L) m^{-2} yr^{-1}) a_{320} (x 10^3)	Reference
9	44	ESS outer shelf	Continuous	9.5	~10–23	0.6	In this study
10	49	ESS outer shelf	Continuous	8.2	~11–27	268	In this study
11	58	ESS outer shelf	Transition zone	394.5	~943–2240	535	In this study
12	65	ESS outer shelf	Discontinuous	19.8	~23–55	45	In this study
15	368	ESS slope	No	9.2	~17–41	11	In this study
14	1350	ESS slope	No	7.8	~9–21	22	In this study
–	52	Laptev Sea shelf	Yes	20–240 (0–48 mbsf)	–	–	Overduin et al., 2015
–	3446–4383	Amundsen and Nansen basins	No	0.5–4.2 (0–10 cmbsf)	from −0.5 to 3.2	–	Rossel et al., 2016
–	1056–5525	Fram Strait	No	1.2–11.4 (0–10 cmbsf)	~1–10	–	Rossel et al., 2020
–	100–2240	Chukchi Sea and ESS slope	No	–	–	from −30 to 66 (a_{350})	Chen et al., 2016

Note: Surface sediment porosity ϕ_o of 0.86 in this study was adopted from a shelf site JCP1 at the neighboring Chukchi Sea* (Chen et al., 2016).
Diffusion coefficient D_s was adjusted from Burdige et al. (1992) with DOM molecular weight ~ 350 Da in this study.

S9 is presumably more influenced by fluvial runoff and coastal erosion from land as supported by correlation between salinity and DOM parameters ($r = 0.39$–0.54, $p < 0.05$, Fig. S3). Likewise, downcore profiles of CDOM absorption coefficients at other sites are relatively stable, except for sites S9 and S10, which showed slightly higher levels at shallow sediments.

To further investigate the characteristics of DOM fluxing from subsea permafrost, we measured MW distributions of seawater and pore water samples (Fig. 6). The DOC concentrations obtained from sum of each fractions are generally consistent with the bulk DOC analysis with TOC analyzer (Table S3), SEC-OCD chromatograph for pore waters featured extremely high low molecular weight (LMW)-dominated DOC (≥ 98%) concentrations at all sites. According to the Eq. (2), LMW DOM has higher diffusion coefficient. LMW DOM (nominal average molecular weight M_n < 350 Da) also prevailed in seawaters at all sites, with 58–62% abundance for surface waters and 62–99% distribution for bottom waters. Seawaters contained relatively more abundances of humic substances (HS) and building blocks (BB) fractions (up to 39%) as compared to pore waters (only 1–2%). Such a LMW-dominated DOM release upon ice melting was also observed in the Arctic previously (Retelletti Brogi et al., 2018). Although permafrost-derived DOM is supposed to contain HS and BB fractions, it can be largely degraded to LMW fractions during millennium time scale, which is in line with the size-reactivity continuum model that LWM fractions are more biorefractory in the ocean (Benner and Amon, 2015).

Efflux from freshly and actively thawing subsea permafrost can be a plausible scenario to explain the extremely high DOC at outer shelf site S11. With seawater depth at ~59 m, this site is located at the transition zone of continuous-discontinuous subsea permafrost (Romanovskii et al., 2005; Shakhova et al., 2019). Since we observed normal DOC levels at other shelf sites with seawater depths at 44 m (S9), 49 m (S10), and 65 m (S12) and also slope sites S14 and S15 (Fig. S5), it can be presumed that the hotspots of DOM venting may be located along a corridor of continuous-discontinuous boundary where subsea permafrost actively thawing and releasing DOM with bottom water temperature at −1.6 °C. Subsea permafrost can be entirely unfrozen even at temperature of −1.8 °C due to very high salt content (Romanovskii et al., 2005) and heat influx. The salinity ranges from 34 to 38 in the measured pore waters (Table S2). Indeed, submerged taliks usually thicken seaward and often deepen at places of outer shelf inundated for a long time period, paleoriver valleys, ice scouring areas (as deep as 10 m), submarine groundwater discharge vents, geological fault zones, etc. (Osterkamp and Harrison, 1985; Rachold et al., 2007; Shakhova et al., 2017; Charkin et al., 2017; Keskitalo et al., 2017). Downward movement of subsea ice-bonded permafrost table has been reported in the Arctic shelf at a rate of ~14 cm yr^{-1} nearshore over the past three decades (Shakhova et al., 2017). We infer that the presumed talik depth where active DOM venting occurs might be placed between 12.5 cm and 20 cm at the site S11 based on the DOC downcore profile, falling within the estimated subsea permafrost annual degradation rate of ~10–30 cm (Razumov, 2000; Romanovskii et al., 2005; Grigoriev, 2008; Shakhova et al., 2017; Shakhova et al., 2019). The depth of subsea permafrost at the study sites are >100 m (Fig. S1). The DOC downcore profiles at shallower sites of S9 and S10 (seawater depth ≤ 49 m) are relatively stable, suggesting relatively stable condition of continuous subsea permafrost. At site S12 (seawater

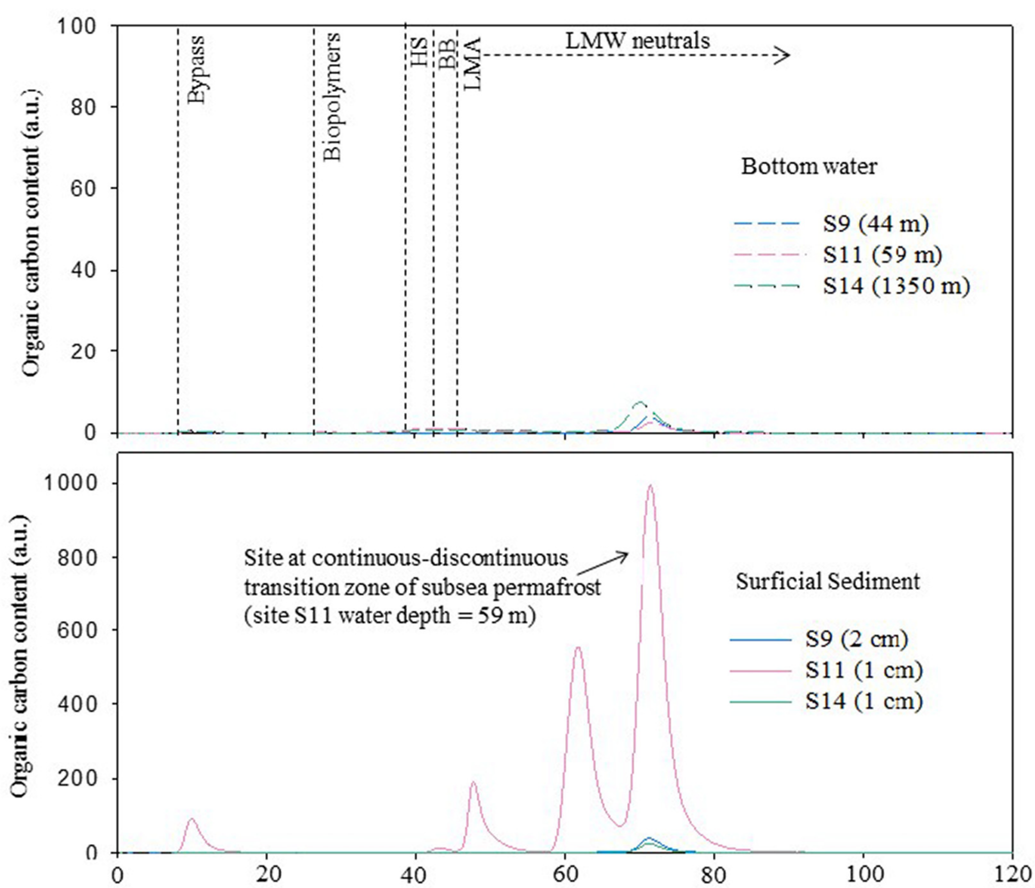

Fig. 6. SEC-OCD chromatographs of DOM from bottom water and pore water in surficial sediment at representative stations. Note the y-axis scale for pore water is 10 times higher than that for bottom water. Biopolymers (M_n > 10 kDa); HS = humic substances (M_n = ~1 kDa); BB = building blocks (M_n = 350–500 Da); LMA = low molecular weight acids (M_n < 350 Da); LMW neutrals (M_n < 350 Da). M_n = nominal average molecular weight ($M_n = \Sigma N_i M_i / \Sigma N_i$, where M_i s the molecular mass and N is the number of molecules). Bypass was to obtain a detector signal at the dead volume time of each run.

Table 2
Estimated benthic flux of DOC fractions in the East Siberian Sea. Positive values denote efflux from sediments and vice versa.

Items	Depth (m)	Bulk (g C m^{-2} yr^{-1})	Fractions (g C m^{-2} yr^{-1})				
		DOC	Biopolymers	Humic substances	Building blocks	LMW acids	LMW neutrals
Site 9	44	~10–23	~0.02–0.06	~0.0–0.1	0	0	~10–23
Site 11	59	~943–2240	~0.09–0.22	~0.4–1.0	~12–28	~63–149	~867–2060
Site 14	1350	~9–21	0.01	−(0.3–0.6)	0	0	~9–22

Diffusion coefficient D_s was adjusted from Burdige et al. (1992) after correcting DOM molecular weight from ~1000 Da to M_n of each fraction.

depth ≥ 65 m) where "patchy" permafrost exists, DOC level decreased from ~20 mg-C L^{-1} to ~11 mg-C L^{-1} at ~20 cmbsf, potentially implying degradation of relic permafrost after active thawing like the neighboring site S11.

3.4. Estimation of benthic effluxes of DOC, CDOM, and FDOM

In this study, a quantitative estimation of benthic diffusion was made based on the Fick's first law and it revealed a potential DOC venting rate of ~943–2240 g C m^{-2} yr^{-1} at site S11 and efflux rates of ~9–55 g C m^{-2} yr^{-1} at remainder shelf sites and slope sites (Table 1). The extremely high efflux rate at site S11 is comparable to a thaw-out release rate of 1600 g C.

m^{-2} yr^{-1} by offshore permafrost observed at a river mouth site on the East Siberian Arctic Shelf underlain with offshore permafrost (Wild et al., 2018). On the other hand, the DOC efflux rates at the remainder sites are comparable to the higher end of those reported in other marine sediments, such as Alaskan Skan Bay (up to 42 g C m^{-2} yr^{-1}, Burdige et al., 1992) and the Arctic Fram Strait (up to 10 g m^{-2} yr^{-1}, Rossel et al., 2020). The efflux rate at discontinuous subsea permafrost site S12 is ~2 times higher than those at sites S9 and S10 with continuous subsea permafrost. In detail, efflux rates of CDOM absorption coefficient a_{320} are 1–3 orders of magnitude higher at sites S11 and S10 at 535,000 and 268,000 (m^{-1} L) m^{-2} yr^{-1}, respectively, than the remainder sites, with the lowest value of 600 (m^{-1} L) m^{-2} yr^{-1} at closer-to-shore site S9. LMW fractions ($M_n < 350$ Da) efflux at rates of ~930–2209 g m^{-2} yr^{-1} at site S11 and 9–23 g m^{-2} yr^{-1} at other sites (Table 2). The FDOM efflux rates for seven components are estimated to range from −2 to 2892 (RU L) m^{-2} yr^{-1} at site S11 (Table 3).

The estimated massive efflux of LMW-dominated DOM from sediments with subsea permafrost, which is usually hundreds of meters in depth (Fig. S1), is very significant from the perspectives of climate change effects on contemporary global carbon cycle considering the large amount of organic carbon stock (~1400 Pg C) in it. Assuming that the width of the swath along the boundary of continuous-discontinuous where subsea permafrost is actively degrading and venting DOM (like site S11) is 1–10 m and this transition zone accounts for approximately 1–10% of the total Arctic subsea permafrost area of 2.5×10^6 km^2 (Angelopoulos et al., 2020), the estimated efflux amount will be 40–400 Tg C yr^{-1} from this transition zone. Furthermore, assuming sites S9 and S10, S11, and S12 representatives of places of isobaths <50 m or < 59 m, ~50–60 m or ~ 59–60 m, and 60–100 m at Arctic shelf, the total annual release of DOM from sediments underlain with offshore permafrost is estimated to be approximately 0.7–1.0 Pg C (i.e., ~700–1000 Tg C, Fig. 8), which is much higher than annual export of ~44 ± 10 Tg C from activated coastal Yedoma (Vonk et al., 2012) and even the total Arctic riverine DOC annual flux to the ocean (25–36 Tg C, Raymond et al., 2007). It is notable that there are several aspects with uncertainties that might lead to inaccurate estimates for the efflux when scaling up to the entire Arctic shelf underlain with subsea permafrost considering the seasonal and spatial heterogeneity. For example, bottom-fast ice can form in winter in some regions and the shelves of the East Siberian and Chukchi Seas are crossed by a major transform fault zone (Bogdanov and Til'man, 1992) where higher efflux rates of DOC may exist. In addition, the Fick's first law only consider the diffusion process while in natural environments current advection and sediment re-suspension can occur. According to the estimated DOC efflux rate of ~0.7–1.0 Pg C yr^{-1}, the Arctic subsea permafrost carbon stock of ~1400 Pg C could be released in ~1400–2000 yrs. keeping the current efflux rates, tallying with the estimation using the subsea permafrost degradation rates of ~10–30 cm yr^{-1}, as aforementioned, assuming an average permafrost depth of ~300 m (Fig. S1, 300 m / ~10–30 cm yr^{-1} = 1000–3000 yrs). Obviously, the benthic efflux rates and the subsea permafrost depth may change with time. Meanwhile, the total area of the subsea permafrost is expected to decrease with some thin permafrost farther offshore thawing out first. This means that the actual benthic efflux amounts could decrease or increase with time depending on the trade-offs between projected increasing efflux rates and shrinking total offshore permafrost area under different scenarios of emission and climate change. The thaw-out time might be longer for some areas with subsea permafrost thicker than 300 m and/or with slower permafrost degradation rates.

3.5. Clustering of shelf pore waters with seawaters from the East Siberian-Chukchi Seas: Implications into subsea permafrost DOM inputs to water column

In order to elucidate DOM sources, PCA was performed based on DOM optical quality data for seawater and pore water samples from the East Siberian-Chukchi Seas (Fig. 7). Datasets from prior studies in the vicinity were also included for better comparison (Fig. 1). Interestingly, there is a clear clustering of pore waters from shelf sites (i.e., S9, S10, S11, and S12) with Arctic seawaters from both the East Siberian and Chukchi seas which is characterized by relatively more enrichment of the red-shifted terrestrial humic-like FDOM $C_{285(370)/>500}$ and more control by aromaticity proxy a^*_{254}, consistent with DOM characteristics originated from sediment-derived permafrost. On one hand, this indicates active interactions between seawaters in the eastern East Siberian-Chukchi Seas and shelf pore waters so they appear to share similar CDOM quality. On the other hand, it could suggest DOM released from sediments with the red-shifted terrestrial humic-like signal (7–8%, Table S2), typical for sediment/soil-derived DOM (Chen et al., 2013),

Table 3
Estimated flux (positive values for efflux and vice versa) of FDOM from sediments to water column in the East Siberian Sea.

Items	Depth (m)	FDOM ((RU L) m^{-2} yr^{-1})						
		$C_{270/302}$	$C_{280/342}$	$C_{310/400}$	$C_{<260(345)/445}$	$C_{285(370)/>500}$	$C_{<260/430}$	$C_{280/310}$
Site 11	59	2892	1277	570	892	364	302	−2
Site 14	1350	−72	−23	−32	−3	−919	−10	29,391
Site 15	368	−54	−62	−64	−51	−89	−3	27,393

Note: bottom waters at sites S9, S10 and S12 are removed as outliers during PARAFAC modeling.

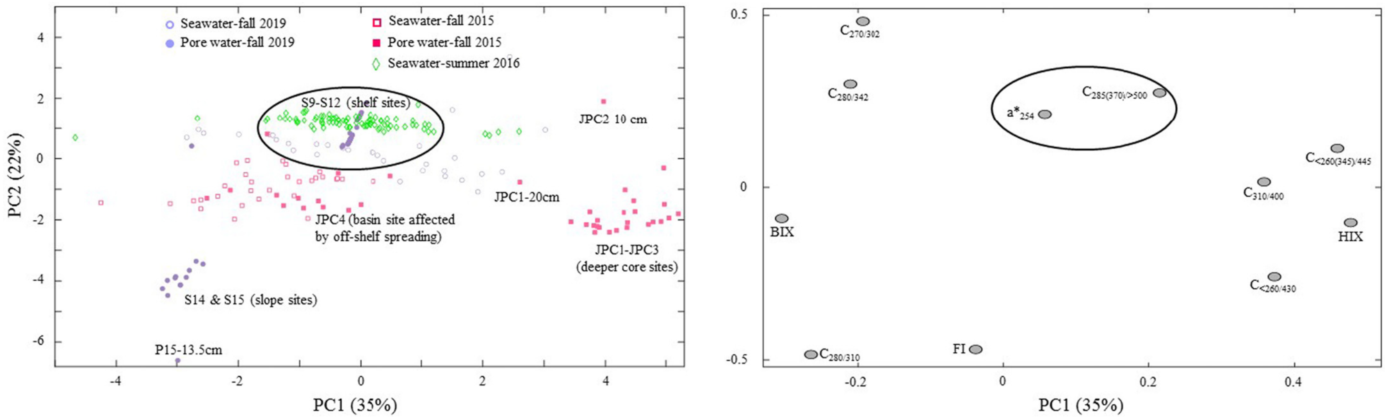

Fig. 7. Principal component analysis (PCA) based on DOM optical data for seawater and sediment pore water samples from the East Siberian-Chukchi Seas of the Arctic Ocean. Pore waters from Arctic shelf underlain with subsea permafrost cluster with seawaters and relatively dominated by aromaticity proxy a^*_{254} and a red-shifted terrestrial humic-like FDOM component $C_{285(370)/>500}$ which is typically relatively enriched in soils and sediments, implying inputs of sediment DOM to water column.

inputs into shelf seawaters (4–6%, Table S1). Although Arctic seas also receive soil/sediment-derived DOM from topsoil via fluvial runoff and coastal Yedoma erosion, the majority of them might have been removed during millennium time scale cross-shelf transport (Tesi et al., 2016; Bröder et al., 2018). Seawaters collected in 2015, when a fall phytoplankton bloom occurred, were distributed closely to seawaters and pore waters in this study and seawaters collected in 2016 but relatively more controlled by protein-like FDOM $C_{280/310}$ and fluorescence index (FI). Pore waters from slope sites at ice-edge are relatively enriched in protein-like component $C_{280/310}$ and FI while pore waters from deeper cores are more controlled by humic-like FDOM. The pore waters from Chukchi Basin site JPC4 were also clustered with 2015 seawaters potentially due to off-shelf spreading of shelf seawater DOM followed by influx of humic substances as seen at slope site S14 (Table 2).

4. Conclusion and environmental implications

Given the huge amount of organic carbon stored in the subsea permafrost and the fast ongoing Arctic warming, accelerating release of small size DOM is projected from the Arctic shelf underlain with offshore permafrost. The estimated benthic efflux rates of DOM ranges from 10 to 2240 g C m^{-2} yr^{-1} and an estimated annual release of

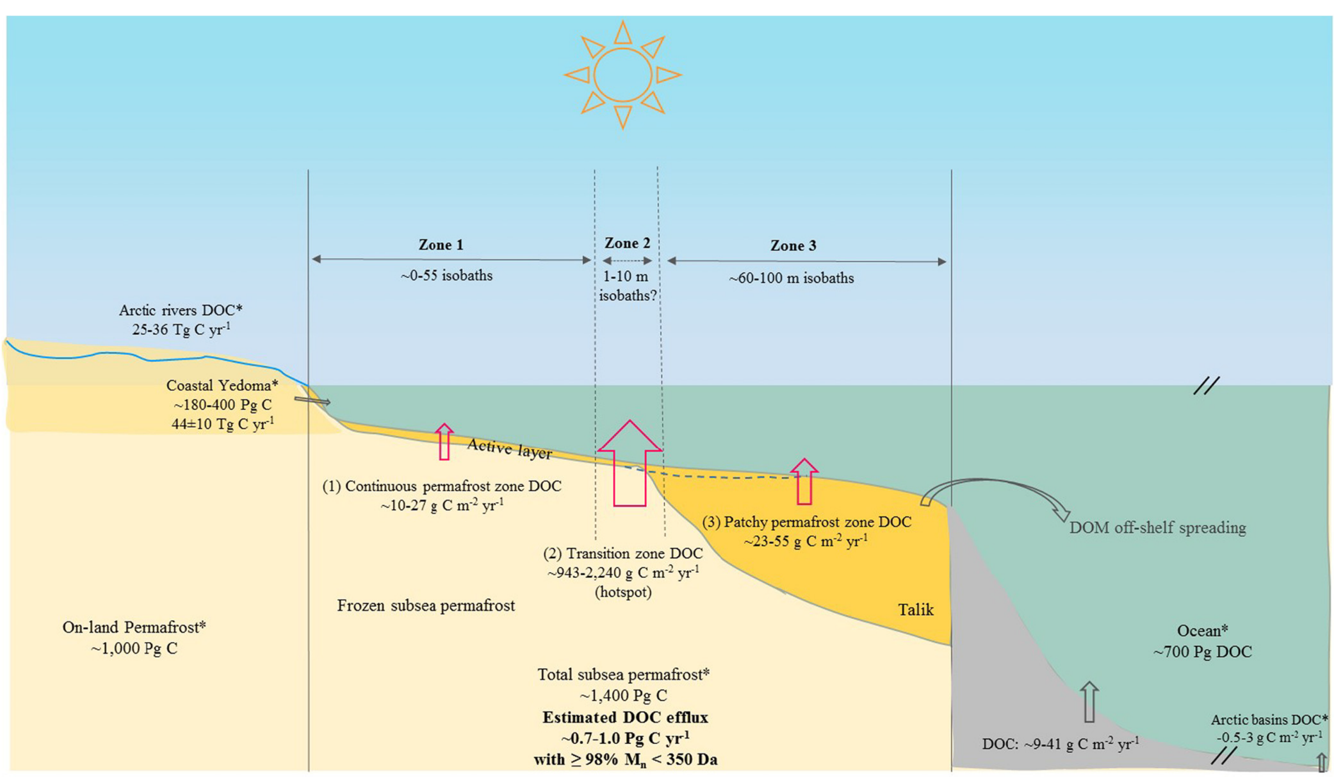

Fig. 8. Conceptual sketch (not to scale) of organic carbon stocks and fluxes around the Arctic shelf underlain with subsea permafrost. Benthic efflux rates: transition zone > > discontinuous zone > continuous zone. Subsea permafrost zones are from Angelopoulos et al. (2019). Carbon stock data regarding permafrost and ocean are from Zimov et al. (2006), Tarnocai et al. (2009), Hugelius et al. (2014), Shakhova et al. (2010), and Jiao et al. (2010). Arctic riverine DOC flux and coastal Yedoma (Ice Complex deposits) organic carbon flux data are from Raymond et al. (2007) and Vonk et al. (2012), respectively. DOC benthic efflux rates at the Arctic basins are from Rossel et al. (2016). Total benthic efflux from region underlain with subsea permafrost are estimated by scaling up via assuming sites S9 and S10, site S11, and site S12 are representative of benthic efflux rates at zone 1, 2, and 3, respectively.

~0.7–1.0 Pg C from the Arctic shelf underlain with offshore permafrost, much higher than total inputs from Arctic rivers and coastal Yedoma, and primary productivity. Dubbed as the "sleeping giants", activation of this dormant old carbon stock could be faster than we previously thought. The estimated huge amount of organic carbon released from the shallow Arctic shelf might potentially exacerbate the carbon inputs to the atmosphere from bubbling Arctic shelf seafloor at present. The Arctic ecosystem responses to the fast release of pre-aged LMW subsea permafrost-derived DOM is unknown at this stage. Moreover, since frozen permafrost can act as a lid to hold the methane inside and below permafrost in place, uncovering of the methane due to thawing permafrost can lead to escape of methane into water column and atmosphere. According to the observed off-shelf spreading phenomena, it is expected that, at least partly, released DOM flows into the Arctic interior via currents such as the Transpolar Drift. The fate of the unlocked DOM, largely depending on its reactivity, is unclear at the moment. However, it is notable that ancient on-land permafrost derived DOM has been found to be sensitive to photo- and subsequent bio-degradation (Cory et al., 2013, 2014). Considering that the Arctic Ocean will be ice-free in summer rather soon, exposure to sunlight may stimulate remineralization of released DOM and exacerbate global warming. More future works are merited to determine the reactivity and fate of subsea permafrost-derived DOM to better understand and predict the carbon-climate feedbacks on Earth.

CRediT authorship contribution statement

Meilian Chen: Data curation, Writing – original draft, Validation. **Ji-Hoon Kim:** Investigation, Resources, Writing - review & editing. **Yun Kyung Lee:** Investigation, Project administration, Validation. **Dong-Hun Lee:** Validation. **Young Keun Jin:** Validation. **Jin Hur:** Funding acquisition, Project administration, Resources, Writing - review & editing.

Declaration of competing interest

The authors declare no competing interest.

Acknowledgements

This work was funded by the Korea Polar Research Institute Grants PM20050 (KIMST Grant 20160247) and NP2018-022. The authors are grateful for helps from caption and crews of *R/V Araon* during the Arctic expedition in 2019.

Appendix A. Supplementary data

Supplementary data to this article can be found online at https://doi.org/10.1016/j.scitotenv.2021.146100.

References

Aksenov, A.A., 1987. Arctic Eurasian Shelf in the Late Quaternary Period. Nauka, Moscow, p. 277.

Anderson, L.G., Jutterstrom, S., Hjalmarsson, S., Wahlstrom, I., Semiletov, I.P., 2009. Outgassing of CO_2 from Siberian Shelf seas by terrestrial organic matter decomposition. Geophys. Res. Lett. 36.

Anderson, L.G., Jorgen, E.K., Ericson, Y., Humborg, C., Semiletov, I., Sundbom, M., Ulfsbo, A., 2017. Export of calcium carbonate corrosive waters from the East Siberian Sea. Biogeosciences 14 (7), 1811–1823.

Angelopoulos, M., Westermann, S., Overduin, P., Faguet, A., Olenchenko, V., Grosse, G., Grigoriev, M.N., 2019. Heat and salt flow in subsea permafrost modeled with CryoGRID2. Journal of Geophysical Research: Earth Surface 124 (4), 920–937.

Angelopoulos, M., Overduin, P.P., Miesner, F., Grigoriev, M.N., Vasiliev, A.A., 2020. Recent advances in the study of Arctic submarine permafrost. Permafr. Periglac. Process. 31 (3), 442–453.

Benner, R., Amon, R.M.W., 2015. The size-reactivity continuum of major bioelements in the ocean. Annu. Rev. Mar. Sci. 7, 2.1–2.21.

Blough, N.V., Del Vecchio, R., 2002. Chromophoric DOM in the coastal environment. In: Hansell, D.A., Carlson, C. (Eds.), Biogeochemistry of Marine Dissolved Organic Matter, 1st Ed. Academic Press, New York, p. 513.

Bogdanov, N.A., Til'man, S.M., 1992. Tectonics and Geodynamics of Northeast of Asia (Explanatory Note to the Tectonic map). p. 54.

Bröder, L., Tesi, T., Andersson, A., Semiletov, I., Gustafsson, O., 2018. Bounding cross-shelf transport time and degradation in Siberian-Arctic land-ocean carbon transfer. Nat. Commun. 9.

Burdige, D.J., Martens, C.S., 1990. Biogeochemical cycling in an organic-rich coastal marine basin: 11. The sedimentary cycling of dissolved, free amino acids. Geochim. Cosmochim. Acta 54 (11), 3033–3052.

Burdige, D.J., Alperin, M.J., Homstead, J., Martens, C.S., 1992. The role of benthic fluxes of dissolved organic carbon in oceanic and sedimentary carbon cycling. Geophys. Res. Lett. 19 (18), 1851–1854.

Charkin, A.N., van der Loeff, M.R., Shakhova, N.E., Gustafsson, Ö., Dudarev, O.V., Cherepnev, M.S., Salyuk, A.N., Koshurnikov, A.V., Spivak, E.A., Gunar, A.Y., Ruban, A.S., Semiletov, I.P., 2017. Discovery and characterization of submarine groundwater discharge in the Siberian Arctic seas: a case study in the Buor-Khaya Gulf, Laptev Sea. Cryosphere 11, 2305–2327.

Chen, M., Maie, N., Parish, K., Jaffé, R., 2013. Spatial and temporal variability of dissolved organic matter quantity and composition in an oligotrophic subtropical coastal wetland. Biogeochemistry 115 (1–3), 167–183.

Chen, M., Kim, J.-H., Nam, S.-I., Niessen, F., Hong, W.-L., Kang, M.-H., Hur, J., 2016. Production of fluorescent dissolved organic matter in Arctic Ocean sediments. Sci. Rep. 6, 39213.

Chen, M., Nam, S.-I., Kim, J.-H., Kwon, Y.-J., Hong, S., Jung, J., Shin, K.-H., Hur, J., 2017. High abundance of protein-like fluorescence in the Amerasian Basin of Arctic Ocean: potential implication of a fall phytoplankton bloom. Sci. Total Environ. 599–600, 355–363.

Chen, M., Jung, J., Lee, Y.K., Hur, J., 2018. Surface accumulation of low molecular weight dissolved organic matter in surface waters and horizontal off-shelf spreading of nutrients and humic-like fluorescence in the Chukchi Sea of the Arctic Ocean. Sci. Total Environ. 639, 624–632.

Chen, M., Kim, J.-H., Hong, S.-W., Lee, Y.K., Kang, M.-H., Jin, Y.-K., Hur, J., 2021. Spectral characterization of dissolved organic matter in seawater and sediment pore water from the Arctic fjords (West Svalbard) in summer. Water 13 (2), 202.

Cory, R.M., Crump, B.C., Dobkowski, J.A., Kling, G.W., 2013. Surface exposure to sunlight stimulates CO_2 release from permafrost soil carbon in the Arctic. Proc. Natl. Acad. Sci. U. S. A. 110 (9), 3429–3434.

Cory, R.M., Ward, C.P., Crump, B.C., Kling, G.W., 2014. Sunlight controls water column processing of carbon in arctic fresh waters. Science 345 (6199), 925–928.

Dmitrenko, I., Kirillov, S., Eicken, H., Markova, N., 2005. Wind-driven summer surface hydrography of the eastern Siberian shelf. Geophys. Res. Lett. 32 (14).

Dmitrenko, I.A., Kirillov, S.A., Tremblay, L.B., Kassens, H., Anisimov, O.A., Lavrov, S.A., Razumov, S.O., Grigoriev, M.N., 2011. Recent changes in shelf hydrography in the Siberian Arctic: potential for subsea permafrost instability. Journal of Geophysical Research: Oceans 116 (C10).

Grigoriev, M.N., 2008. Cryomorphogenesis and Lithodynamics of the Coastal-shelf Zone of the Seas of Eastern Siberia. Doctoral dissertation, Yakutsk Melnikov Permafrost Institute.

Günther, F., Overduin, P.P., Sandakov, A.V., Grosse, G., Grigoriev, M.N., 2013. Short- and long-term thermo-erosion of ice-rich permafrost coasts in the Laptev Sea region. Biogeosciences 10 (6), 4297–4318.

Huber, S.A., Balz, A., Abert, M., Pronk, W., 2011. Characterisation of aquatic humic and non-humic matter with size-exclusion chromatography–organic carbon detection–organic nitrogen detection (LC-OCD-OND). Water Res. 45 (2), 879–885.

Hugelius, G., Strauss, J., Zubrzycki, S., Harden, J.W., Schuur, E.A.G., Ping, C.L., Schirrmeister, L., Grosse, G., Michaelson, G.J., Koven, C.D., O'Donnell, J.A., Elberling, B., Mishra, U., Camill, P., Yu, Z., Palmtag, J., Kuhry, P., 2014. Estimated stocks of circumpolar permafrost carbon with quantified uncertainty ranges and identified data gaps. Biogeosciences 11 (23), 6573–6593.

Jessen, S., Holmslykke, H.D., Rasmussen, K., Richardt, N., Holm, P.E., 2014. Hydrology and pore water chemistry in a permafrost wetland, Ilulissat, Greenland. Water Resour. Res. 50 (6), 4760–4774.

Jiao, N., Herndl, G.J., Hansell, D.A., Benner, R., Kattner, G., Wilhelm, S.W., Kirchman, D.L., Weinbauer, M.G., Luo, T., Chen, F., Azam, F., 2010. Microbial production of recalcitrant dissolved organic matter: long-term carbon storage in the global ocean. Nat Rev Micro 8 (8), 593–599.

Keskitalo, K., Tesi, T., Broder, L., Andersson, A., Pearce, C., Skold, M., Semiletov, I.P., Dudarev, O.V., Gustafsson, O., 2017. Sources and characteristics of terrestrial carbon in Holocene-scale sediments of the east Siberian Sea. Clim. Past 13 (9), 1213–1226.

Lantuit, H., Overduin, P.P., Couture, N., Wetterich, S., Aré, F., Atkinson, D., Brown, J., Cherkashov, G., Drozdov, D., Forbes, D.L., Graves-Gaylord, A., Grigoriev, M., Hubberten, H.-W., Jordan, J., Jorgenson, T., Ødegård, R.S., Ogorodov, S., Pollard, W.H., Rachold, V., Sedenko, S., Solomon, S., Steenhuisen, F., Streletskaya, I., Vasiliev, A., 2012. The Arctic coastal dynamics database: a new classification scheme and statistics on Arctic permafrost coastlines. Estuar. Coasts 35 (2), 383–400.

Lobbes, J.M., Fitznar, H.P., Kattner, G., 2000. Biogeochemical characteristics of dissolved and particulate organic matter in Russian rivers entering the Arctic Ocean. Geochim. Cosmochim. Acta 64 (17), 2973–2983.

Nicolsky, D., Shakhova, N., 2010. Modeling sub-sea permafrost in the East Siberian Arctic Shelf: the Dmitry Laptev Strait. Environ. Res. Lett. 5 (1), 015006.

Nikiforov, E.G., Shpaikher, A.O., 1980. Features of the Formation of Hydrological Regime Large-scale Variations in the Arctic Ocean. Leningrad, Hydrometeoizdat, p. 269.

Osterkamp, T.E., Harrison, W.D., 1985. Subsea Permafrost: Probing, Thermal Regime and Data Analyses, Report UAGR-301. Geophysics Institute, University of Alaska, Fairbanks.

Overduin, P.P., Liebner, S., Knoblauch, C., Günther, F., Wetterich, S., Schirrmeister, L., Hubberten, H.-W., Grigoriev, M.N., 2015. Methane oxidation following submarine

permafrost degradation: measurements from a Central Laptev Sea shelf borehole. Journal of Geophysical Research: Biogeosciences 120 (5), 965–978.
Perrette, M., Yool, A., Quartly, G.D., Popova, E.E., 2011. Near-ubiquity of ice-edge blooms in the Arctic. Biogeosciences 8 (2), 515–524.
Rachold, V., Grigoriev, M.N., Are, F.E., Solomon, S., Reimnitz, E., Kassens, H., Antonow, M., 2000. Coastal erosion vs riverine sediment discharge in the Arctic Shelf seas. Int. J. Earth Sci. 89 (3), 450–460.
Rachold, V., Eicken, H., Gordeev, V.V., Grigoriev, M.N., Hubberten, H.-W., Lisitzin, A.P., Shevchenko, V.P., Schirrmeister, L., 2004. Modern Terrigenous Organic Carbon Input to the Arctic Ocean. In: Stein, R., MacDonald, R.W. (Eds.), The Organic Carbon Cycle in the Arctic Ocean. Springer Berlin Heidelberg, Berlin, Heidelberg, pp. 33–55.
Rachold, V., Bolshiyanov, D.Y., Grigoriev, M.N., Hubberten, H.-W., Junker, R., Kunitsky, V.V., Merker, F., Overduin, P., Schneider, W., 2007. Nearshore arctic subsea permafrost in transition. Eos, Transactions American Geophysical Union. 88(13), pp. 149–150.
Raymond, P.A., McClelland, J.W., Holmes, R.M., Zhulidov, A.V., Mull, K., Peterson, B.J., Striegl, R.G., Aiken, G.R., Gurtovaya, T.Y., 2007. Flux and age of dissolved organic carbon exported to the Arctic Ocean: a carbon isotopic study of the five largest arctic rivers. Glob. Biogeochem. Cycles 21 (4), GB4011.
Razumov, S.O., 2000. Rates of coastal thermoabrasion as a function of climate and morphological characteristics of the coast. Geomorphology 3, 88–94.
Retelletti Brogi, S., Ha, S.-Y., Kim, K., Derrien, M., Lee, Y.K., Hur, J., 2018. Optical and molecular characterization of dissolved organic matter (DOM) in the Arctic ice core and the underlying seawater (Cambridge Bay, Canada): implication for increased autochthonous DOM during ice melting. Sci. Total Environ. 627, 802–811.
Rivchter-Menge, J., Druckenmiller, M.L., Jeffries, M., 2019. Arctic Report Card. http://www.arctic.noaa.gov/reportcard.
Romanovskii, N.N., Hubberten, H.W., Gavrilov, A.V., Eliseeva, A.A., Tipenko, G.S., 2005. Offshore permafrost and gas hydrate stability zone on the shelf of East Siberian Seas. Geo-Mar. Lett. 25 (2), 167–182.
Rossel, P.E., Bienhold, C., Boetius, A., Dittmar, T., 2016. Dissolved organic matter in pore water of Arctic Ocean sediments: environmental influence on molecular composition. Org. Geochem. 97, 41–52.
Rossel, P.E., Bienhold, C., Hehemann, L., Dittmar, T., Boetius, A., 2020. Molecular composition of dissolved organic matter in sediment porewater of the Arctic Deep-Sea observatory HAUSGARTEN (Fram Strait). Front. Mar. Sci. 7 (428).
Sakshaug, E., 2004. Primary and secondary production in the Arctic seas. In: Stein, R., Macdonald, R.W. (Eds.), The Organic Carbon Cycle in the Arctic Ocean. Springer-Verlag, Heidelberg, pp. 57–82.
Salvadó, J.A., Tesi, T., Sundbom, M., Karlsson, E., Kruså, M., Semiletov, I.P., Panova, E., Gustafsson, Ö., 2016. Contrasting composition of terrigenous organic matter in the dissolved, particulate and sedimentary organic carbon pools on the outer East Siberian Arctic Shelf. Biogeosciences 13 (22), 6121–6138.
Schlitzer, R., 2020. Ocean Data View. http://odv.awi.de.
Semiletov, I., Dudarev, O., Luchin, V., Charkin, A., Shin, K.-H., Tanaka, N., 2005. The East Siberian Sea as a transition zone between Pacific-derived waters and Arctic shelf waters. Geophys. Res. Lett. 32 (10), L10614.
Semiletov, I., Pipko, I., Gustafsson, O., Anderson, L.G., Sergienko, V., Pugach, S., Dudarev, O., Charkin, A., Gukov, A., Broder, L., Andersson, A., Spivak, E., Shakhova, N., 2016. Acidification of East Siberian Arctic Shelf waters through addition of freshwater and terrestrial carbon. Nat. Geosci. 9 (5), 361–367.
Shakhova, N., Semiletov, I., Salyuk, A., Yusupov, V., Kosmach, D., Gustafsson, Ö., 2010. Extensive methane venting to the atmosphere from sediments of the East Siberian Arctic Shelf. Science 327 (5970), 1246–1250.
Shakhova, N., Semiletov, I., Gustafsson, O., Sergienko, V., Lobkovsky, L., Dudarev, O., Tumskoy, V., Grigoriev, M., Mazurov, A., Salyuk, A., Ananiev, R., Koshurnikov, A., Kosmach, D., Charkin, A., Dmitrevsky, N., Karnaukh, V., Gunar, A., Meluzov, A., Chernykh, D., 2017. Current rates and mechanisms of subsea permafrost degradation in the East Siberian Arctic Shelf. Nat. Commun. 8 (1), 15872.
Shakhova, N., Semiletov, I., Chuvilin, E., 2019. Understanding the permafrost–hydrate system and associated methane releases in the East Siberian Arctic Shelf. Geosciences 9 (6), 251.
Soloviev, V.A., Ginzburg, G.D., Telepnev, E.V., Mikhaluk, Y.N., 1987. Cryothermia of Gas Hydrates in the Arctic Ocean. VNIIOkeangeologia.
Stein, R., Macdonald, R.W., 2004. The Organic Carbon Cycle in the Arctic Ocean. Springer, Heidelberg, Germany.
Tarnocai, C., Canadell, J.G., Schuur, E.A.G., Kuhry, P., Mazhitova, G., Zimov, S., 2009. Soil organic carbon pools in the northern circumpolar permafrost region. Glob. Biogeochem. Cycles 23 (2), GB2023.
Tesi, T., Semiletov, I., Dudarev, O., Andersson, A., Gustafsson, O., 2016. Matrix association effects on hydrodynamic sorting and degradation of terrestrial organic matter during cross-shelf transport in the Laptev and East Siberian Shelf seas. Journal of Geophysical Research-Biogeosciences 121 (3), 731–752.
Vetrov, A.A., Romankevich, E.A., 2004. Carbon Cycle in the Russian Arctic Seas. Springer, Berlin.
Vetrov, A.A., Romankevich, E.A., 2011. Primary production and fluxes of organic carbon to the seabed in the Russian Arctic seas as a response to the recent warming. Oceanology 51 (2), 255–266.
Vonk, J.E., Sanchez-Garcia, L., van Dongen, B.E., Alling, V., Kosmach, D., Charkin, A., Semiletov, I.P., Dudarev, O.V., Shakhova, N., Roos, P., Eglinton, T.I., Andersson, A., Gustafsson, O., 2012. Activation of old carbon by erosion of coastal and subsea permafrost in Arctic Siberia. Nature 489 (7414), 137–140.
Vonk, J.E., Semiletov, I.P., Dudarev, O.V., Eglinton, T.I., Andersson, A., Shakhova, N., Charkin, A., Heim, B., Gustafsson, O., 2014. Preferential burial of permafrost-derived organic carbon in Siberian-Arctic shelf waters. J. Geophys. Res. Oceans 119 (12), 8410–8421.
Wild, B., Shakhova, N., Dudarev, O., Ruban, A., Kosmach, D., Tumskoy, V., Tesi, T., Joß, H., Alexanderson, H., Jakobsson, M., Mazurov, A., Semiletov, I., Gustafsson, Ö., 2018. Organic matter across subsea permafrost thaw horizons on the East Siberian Arctic Shelf. The Cryosphere Discuss. 2018, 1–26.
Woodgate, R.A., Aagaard, K., Swift, J.H., Falkner, K.K., Smethie Jr., W.M., 2005. Pacific ventilation of the Arctic Ocean's lower halocline by upwelling and diapycnal mixing over the continental margin. Geophys. Res. Lett. 32 (18).
Zimov, S.A., Schuur, E.A.G., Chapin, F.S., 2006. Permafrost and the Global Carbon Budget. Science 312 (5780), 1612–1613.